Energy Proceedings
2022
ISSN 2004-2965

Biogeochemical Footprints In Variant Methane Seepage Intensity Reveal Methane Ultimate Fate In Cold Seep#

Hui zhang[1,2,3,4], Jingchun Feng[1,2,3,4*], Yongming Shen[1,2,3,4], Li Tang[1,2,4], Zhifeng Yang[1,2,3,4], Si Zhang[1,2]

1 Research Centre of Ecology & Environment for Coastal Area and Deep Sea, Guangdong University of Technology & Southern Marine Science and Engineering Guangdong Laboratory (Guangzhou), Guangzhou, 510006, China

2 Southern Marine Science and Engineering Guangdong Laboratory (Guangzhou), Guangzhou, 511458, China

3 Guangdong Provincial Key Laboratory of Water Quality Improvement and Ecological Restoration for Watersheds, Institute of Environmental and Ecological Engineering, Guangdong University of Technology, Guangzhou, 510006, China

4 School of Ecology, Environment and Resources, Guangdong University of Technology, Guangzhou, 510006, China

ABSTRACT

Methane seepages from natural process or gas hydrate dissociation are proposed to cause adverse effect of climate change. The ultimate fate of methane leakage from the deep sea is less understood. Here, a systematic investigation of dissolved methane intensity, characteristic of pore fluid migration, metallogenic features of the sediment, and evolutions of biological communities in different methane seeping areas was conducted by high-resolution image, pore fluid geochemical analysis, and lithologic and surface analysis of the sediment. Results indicate that with high methane flux, biogeochemical progresses dominated by AOM in sediments, excess methane emissions to seawater and the methane metabolic communities dominate. While at low methane fluxes, AOM co-exists with OSR. This work reveals the dynamic marine methane cycle mechanism in different seepage intensities.

Keywords: natural gas hydrate, methane seepage intensity; biogeochemical footprints, community succession sequence

1. INTRODUCTION

Marine sediment is regarded as the largest methane pool because of the huge amount of methane trapped in the solid form of nature gas hydrate (NGH) [1]. Once the NGH was dissociated or dissolved with the destabilization of pressure, temperature, or chemical composition change, methane bubbles or methane-bearing fluids migrate continually upward to the seafloor and water column.

NGH is a promising clean energy, because the large amount of methane trapped in NGH is conducive to decarbonization of the traditional fossil energy system. Nevertheless, methane is also one of the greenhouse gases, which has 28 times the global warming power of carbon dioxide [2, 3]. Hence, rational exploitation of NGH and uncovering the geological and environmental footprint of methane release play significant role in the low-carbon energy transition and dealing with climate change [4]. Abundant evidence shows that significant quantities of methane were released into the atmosphere, triggered by large amounts of NGH dissociation in the paleoclimatic events [5, 6]. Not only that, massive and uncontrollable NGH dissociation causes the deep-sea landslides, deep-sea volcanic activity, huge amounts of methane emitting to the atmosphere, and other geological hazards [7, 8]. However, in the majority of cases, for continuous and controllable methane release at the seafloor, the majority of methane was converted anaerobically, fueling the flourishing chemosynthetic cold seep ecosystem, and leads to less than 10% of the released methane can be transported into the atmosphere [9]. Therefore, to understand the dynamic marine methane cycle mechanism, clarifying the characteristics of geochemical evolution associated with ecosystem development at different stages of methane release at the seafloor are essential.

Currently, sulfate-driven methane anaerobic oxidation reaction (S-AOM) is regarded as the main methane oxidation pathway in marine sediments [10]. The following reaction is the result of the combined action of sulfate-reducing bacteria and methane oxidizing archaea [11, 12]:

This is a paper for the 8th Applied Energy Symposium - CUE2022, Sept. 24-27, 2022, Matsue, Japan.

*Corresponding author. E-mail address: fengjc@gdut.edu.cn (J.C. Feng) Tel: +86-20-39322141; fax: 020-39322141

$$CH_4 + SO_4^{2-} \rightarrow HCO_3^- + HS^- + H_2O \quad (1)$$

Such reaction releases HCO_3^- and HS^- while consuming methane and sulfate. In addition, the organic matter sulfate reduction is typical biogeochemical process in normal marine sediments by sulfate-reducing bacteria to generates HCO_3^- and H_2S while use organic matter [13, 14]:

$$2CH_2O + SO_4^{2-} \rightarrow 2HCO_3^- + H_2S \quad (2)$$

The rates of sulfate consumption by OSR and AOM were variation in different regions [15]. In active methane seeps, massive methane emission from sediments. Sulfate was heavily consumed by the interaction of AOM, more HCO_3^- and HS^-released to pore fluids [16]. The AOM in sediments be called filter for methane in the ocean. Furthermore, these reactions usually result in authigenic minerals and has an impact on the migration and transformation of metal ions in pore fluids. In contrast, the AOM was weak in areas with inactive methane seeps, ion migration in pore fluids and authigenic minerals in sediments are mainly influenced by early diagenesis. Methane leakage level will result in AOM with varying intensities in sediments at various stages of cold seep development, which will change the mineral composition of the sediments and ion concentration in pore fluid. Formation of different chemosynthetic ecosystems that use sulfide and methane in pore fluids for food, with the change in released upward fluid components and the geological conditions there. Those progress contributed to biogeochemical cycles. Clearly, it is important to developing full understanding of the biogeochemical footprint of methane leakage in this methane filter for better regulation of contemporary climate change and resource development of gas hydrates.

Methane seepage fields where hydrocarbon-rich fluids are transported upward to form cold seep. The “Haima” cold seep in the northern part of the South China Sea is the second active methane cold seep discovered in China. Compared with the Formosa cold seep, the “Haima” cold seep has a larger range and a higher resource reserve. Previous studies about “Haima” cold seep have focused on the geochemical processes and elemental cycling, or investigated the biological characteristics of biomes [17-24]. Nevertheless, our understanding of the characteristics of geochemical evolution associated with ecosystem development at different stages of methane release at the seafloor in this area remains scarce.

The present study investigated the various biogeochemical footprint of pore fluids that in different stages of methane emissions, combined with the evolution of the ecosystem. Due to the biogeochemical characteristics of pore fluids can only represent current characteristics, whereas more persistent presence of sediments presence allows it to preserve the biogeochemical footprint over a wider historical time scale [25], we integrated with physical and chemical properties of sediment in this study. Here, we revealed the effects of methane leakage level on metal ion migration in pore fluids and authigenic mineral composition in sediments and its coupling relationship with ecosystem evolution. Our results will offer new knowledge about biogeochemical progress in sediments with different methane seepage intensity and their potential roles in communities succession sequence for the “Haima” seep.

2. MATERIAL AND METHODS

2.1 Geological Settings and sampling

The Qiongdongnan Basin has favorable geology and NGH source conditions [26]. High purity gas hydrate samples were found in the Qiongdongnan Basin in 2015. The “Haima” cold seep was discovered in 2016, an active cold seep of remarkable size by the Guangzhou Marine Geological Survey. Then, it has also been found that the signature cold seep characteristics, including chemoautotrophic faunal communities, bubble plumes, and abundant authigenic carbonates deposits [19, 27, 28]. A flat topography shows at “Haima” cold seep hence it is unlikely that any recent rapid sedimentary events have occurred. The temperature of the bottom water at“Haima” cold seep of approximately 4°C.

Two sites with different cold seep conditions were selected for sampling in the “Haima” cold seep. The water depth at the Ⅰ and Ⅱsampling sites are 1394 m and 1441 m. The site Ⅰ without the chemoautotrophic megafauna or methane bubbles, which was in early stage of cold seep. The site Ⅱ was in active stage and share some characteristics with those from both active seeps in other parts of the world, including bubble plumes were discovered, and observed the high densities of seep-associated taxa, like bathymodiolin mussels. Therefore, the two sites will naturally show various methane intensity in marine sediments, which enables us to develop a hypothesis about different cold seep development stages.

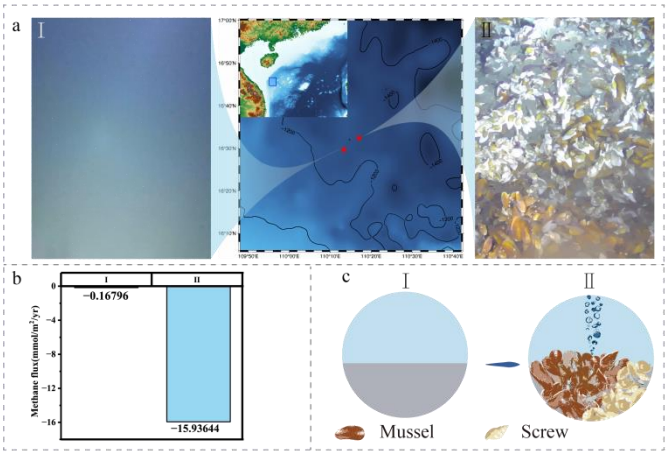

Fig. 1 (a) Locations of sampling sites and characteristics of ecological communities captured by ROV; (b) methane fluxes in sediments at two stations; (c) Schematic diagram of ecological community development at two stations

Gravity cores were taken by a cruise in May 2021 utilizing a gravity piston sampler at those four sites and by Rhizon samplers with pore diameter of 0.2 μm for pore waters. With increasing depth of sediments, the sampling interval rises, and the deep sampling interval under 2 m is 50 cm. Pore waters were kept at 4°C until analysis. The sediment was sampled at the same interval with the pore water, and the samples were freeze-dried and ground in an agate morta.

2.2 Analytical methods

Pore fluids: The pore water samples were tested for Ca^{2+}, Mg^{2+} concentrations using inductively coupled plasma emission spectrometer （ ICP-OES), (Thermo Fisher, ICAP 7000 SERIES). The pore water samples were tested for Fe, Mn ions concentrations by inductively coupled plasma mass spectrometer (ICP-MS), (Thermo Fisher, ICAP RQ). Ion chromatography (Thermo Fisher, Aquion) was used to test SO_4^{2-} concentrations in pore water samples. The pore water samples were tested for TOC (Total organic carbon) and DIC (Dissolved inorganic carbon) concentrations by total organic carbon analyzer (SHIMADZU, TOC-L).

Sediments: The sediment powder was thoroughly ground and screened with a 200-mesh stainless steel screen and scanned with an X-ray diffraction (Rigaku Miniflex-600) in the range of 3–80°. Sediment samples were tested for TOC and DIC concentrations by total organic carbon analyzer (SHIMADZU, TOC-L). Sediment Particle Size distributions were measured using Laser Particle Size Analyzer (Malvern, Mastersizer 3000). The morphology and elemental mapping of the sediments were analyzed on scanning electron microscopes (Tescan, LYRA 3 XMU).

Concentration of methane: The methane concentration in the pore water was determined by injecting 600 μL aliquot of the headspace into a gas chromatography instrument (TRACE 1300, Thermo Scientific) equipped with a Molesieve column. The carrier gas was argon, and the column temperature was 60℃.

2.3 Methane flux calculation

Methane concentration profiles in the sediment were used to compute methane fluxes in the sediment. Methane flux is calculated by Fick's first law [29]:

$$F = -\varphi \times D_{Ca} \times \left(\frac{dC}{dz} \right) \quad (3)$$

where ϕ is the porosity of the sediment. The first derivative of linear regression based on the gradient of pore fluids in the sediments is used to calculate dC/dz [29]. DCH4 is the diffusion coefficient of methane in pore fluids, which is corrected for sediment tortuosity using the equation [30]:

$$D_{CH_4} = D_0 / (1 - \ln(\varphi^2)) \quad (4)$$

where D_0, is the coefficient of methane diffusion in surface sediments in seawater, under the assumption of an average temperature of 4℃.

3. MATERIAL AND METHODS

3.1 Low methane flux drives deeper AOM onset

The site I as depicted in Fig. 1a, seafoor's image show that there was absence of all mega-epifauna, there was also absence of bacterial mats or chemolithoautotrophic communities across a wide range. Which indicated that site I was in the early stages of seep community development.

Less than 1 μM of methane concentration within 0–700 cm in the sediments at site I indicated that the low methane flux in this region. The methane flux diffused from sediments into seawater calculated by Fick's first law was 0.17 mmol/m^2/yr (Fig. 1b). Site I was in an early stage with low intensity methane seepage.

Metal ions migration in pore fluids were impacted by the distinct biogeochemical progress in high-flux environments. Consumption of reactants in pore fluids and the enrichment of reaction product will produce carbonate rocks, pyrite, and other AOM associated minerals, as well as the dissolution and crystallization of barite, changing the mineral fraction of the sediment. As shown in Fig. 2c, the mineral components of the sediment were calculated by using the K-value method on XRD pattens [31]. The sediments mineral composition

at site I were mainly composed of clinochlore and illite, indicating that the sediments are primarily derived from river inputs from Taiwan rather than volcanic ash from Luzon [32]. The terrigenous inputs from Luzon are primarily composed of montmorillonite and kaolin. Although illite can also formed by montmorillonite dehydration which usually happens above 60℃ [33]. Crystallization frequently results in the formation of small amounts of gypsum and halite when sample dried. Feldspar and amphibole are two typical rock-forming minerals, and anomalous changes in the climate typically have an impact on how they are deposited. It has been well documented that the carbonate and pyrite are two typical authigenic mineral of AOM [34]. At site I, XRD patterns of sediments at 2.5 cm and 625 cm depth showed clear calcite (JCPDS Card No.05-0586) peaks at 29.4°, while sediments at 425 cm were almost free of calcite. Insignificant pyrite (JCPDS Card No.42-1340) peaks at 33.08° appeared only in sediments at 425 cm and 625 cm depth.

Early diagenesis mainly occurred at the top layer (0–400 cm depth) of the sediments. Fe/Mn oxide or hydroxide serves as the electron acceptor with higher free energy than SO_4^{2-} of organic matter reduction reaction. Fe/Mn oxide or hydroxide are consumed by metal organic matter reduction reaction (OMR), releasing large amounts of Fe/Mn ions, and the reaction rate was limited by the Fe/Mn oxide or hydroxide contents in sediment as depth increases, as a result that unique Fe/Mn ions concentration profiles in pore water. And DIC was released into the pore fluids and reacts with Ca^{2+} and Mg^{2+} in pore water to produce authigenic carbonate precipitation. Resulting in a high content of calcite in the surface sediment (16.5%). Due to the high intense material exchange between bottom water and surface sediment, Ca^{2+} and Mg^{2+} are constantly replenished from bottom water, and the Fe/Mn ions released by the OMR diffused to bottom water.

Sulfate is more abundant in seawater even though it has a lower free energy than Fe/Mn oxide or hydroxide as an electron acceptor. With Fe/Mn oxides or hydroxides were gradually depleted, and sulfate takes their place as the electron acceptor for reducing organic matter. The SO_4^{2-} concentration at pore fluids ranged from 20 mM to 15 mM in the surface layer (0–400 cm) may be the result of the OSR. Limited by the amount of organic matter, OSR often occurs in the shallow surface of sediments, and the reactivity becomes weaker with the increasing of depth [35]. With the depth increasing, the OSR reaction slows down due to the amount of active organic matter gradually declines. At the same time, HCO_3^- and H_2S were released during the OSR. In the range of 200–400 cm, DIC concentration increased slightly and accompanied by a small consumption of Ca^{2+} and Mg^{2+} in pore fluids, and a small amount of carbonate precipitates were produced. SO_4^{2-} concentration declined in pore fluid below 425 cm, from 16 mM at 425 cm to 7 mM at 775 cm, while DIC concentration also rose quickly below 425 cm. Indicated that below 425 cm in sediment of site I, the decreased SO_4^{2-} concentration in pore water was primarily attributed to the AOM instead of OSR. There are three factors here. Fist, as a general rule, OSR occurs at the shallow surface of sediments, constrained by the amount of organic matter that is readily available, and the reactivity weakens with depth. The OSR was attenuated with increasing depth. Second, the OSR reaction consumes TOC, but TOC content has a pattern of quick accumulation at this range. Third, the bottom has higher methane concentrations than the top sediments.

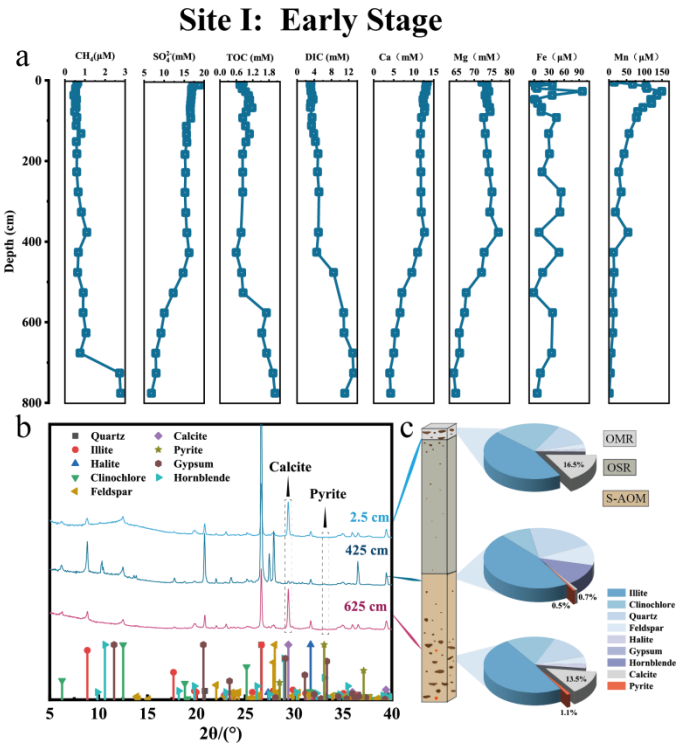

Fig. 2 Ion concentration of pore waters and mineral fraction of sediments at site I*. (a) concentration of metal ions, methane, sulfate, organic carbon, and inorganic carbon in pore fluids; (b) XRD patterns of sediments at depths of 2.5 cm, 425 cm, and 625 cm; (c) mineral composition of sediments at depths of 2.5 cm, 425 cm, and 625 cm.*

Around 425 cm depth, the SO_4^{2-} concentrations profile displayed a severe kink. The formation of kink-type features presupposes two sediments with different SO_4^{2-} profiles sliding against each other. The unusually sharp kink indicated that the event was very recently [36]. Based on SO_4^{2-} profile characteristics, it is hypothesized that there are two stages of SO_4^{2-} consumption. The first

stage was within 425–575 cm, which rapid depletion of SO_4^{2-} in pore fluids. The rate of SO_4^{2-} consumption begins to slow down below 575 cm in the sediment due to the limitation of sulfate concentration. Methane seepage intensity is a significant impact of the biogeochemical footprint in the sediments, and the sulfate profile in steady-state diffusion control systems is linear. This concave sulfate profile may be due to the methane flux variation on time scales [36, 37]. Additionally, geological processes like erosion may result in the formation of a concave sulphate profile. The lower concave sulfate profile illustrates the erratic conditions in the dynamic sedimentary environment, to sum up. Low methane flux and continuous methane depletion by AOM lead to low methane concentration in the pore fluid at site I. Below 425 cm depth, the AOM releases a large amount of HCO_3^- into the pore fluid to react with Ca^{2+} to produce a large amount of authigenic calcite. This process consumes Ca^{2+} in the pore fluids and resulting in an increase of the Mg/Ca ratio, with increasing rates of Mg/Ca ratio, which may lead to the formation of high-magnesium calcite. Lower amount of calcium carbonate precipitation at the early stage of AOM was the cause of the low calcite content at depths of 400–500 cm. Deeper at site I, the enrichment of HCO_3^-in pore water of sediments owing to the AOM will promote cold seep carbonate precipitation. Additionally, carbonate precipitation was inhibited by sulfate, and this inhibition was lessened as the concentration of sulfate decreases. The carbonate content at the bottom was significantly rose and reached 13.5% as DIC concentration accumulated with depth. AOM lead to sulfide builds up in pore water at a rapid rate, and the surplus H_2S generates significant amounts of intermediate molecules, such as sulfur. However, the intermediate was unstable and first produces FeS. With the release of HS^- in excess, the FeS is converted to pyrite, as a result that pyrite minerals appear in the bottom sediment [38-40].

In short, site I with low methane flux, AOM occurs only at the bottom of sediment, and there were no epifaunal communities at the sediment seawater interface, indicating that site I was in the early cold seep stage.

3.2 High methane flux drives shallow AOM oneset

At the site Ⅱ, bubble plumes could be seen clearly, which indicate that established methane-rich fluid flow here. And observed the high densities of seep-associated taxa, contained Mytilidae, Ophiuridae, Turridae, Galatheidae, Alvinocarididae, Lithodidae, and other organisms. Among them, bathymodiolin mussels have higher populations than others.

Mineral composition of sediments at site Ⅱ were mainly composed of clinochlore and illite, too. XRD patterns of the sediments at 2.5 cm, 425 cm, and 625 cm depth both showed clear calcite peaks, shown at Fig.5b, indicated the presence of calcite, and faint peaks of pyrite are present at different depths.

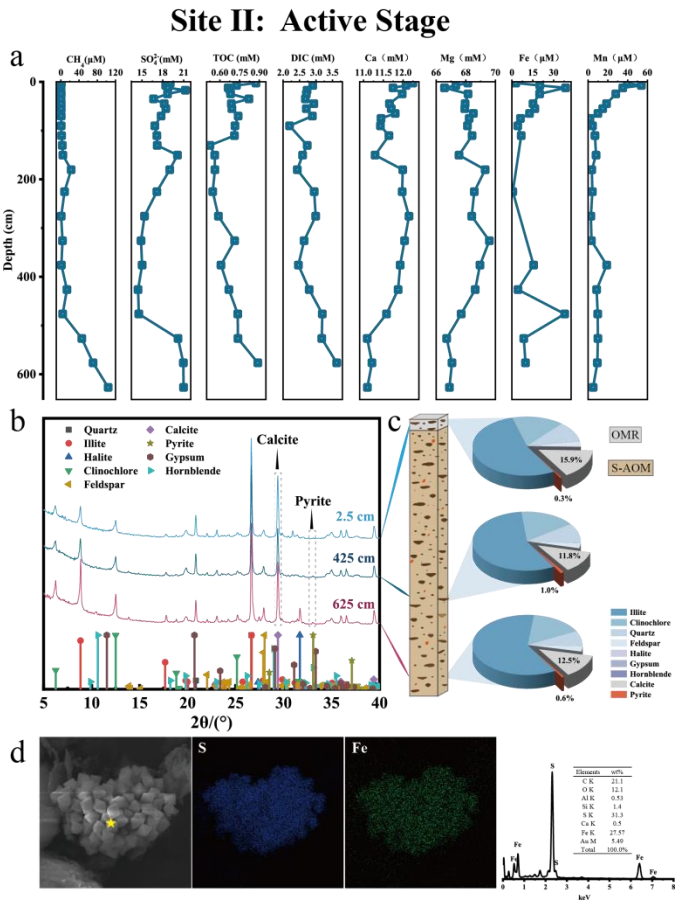

Fig. 3 Ion concentration of pore waters and mineral fraction of sediments at site Ⅱ. (a) concentration of metal ions, methane, sulfate, organic carbon, and inorganic carbon in pore fluids; (b) XRD patterns of sediments at depths of 2.5 cm, 425 cm, and 625 cm; (c) mineral composition of sediments at depths of 2.5 cm, 425 cm, and 625 cm. (d) corresponding EDXS elemental mapping images.

Bioerosion impacted the geochemical processes in the shallow sediment when there was active life above the sediment. In the range of 0–100 cm depth at site Ⅱ, a large amount of Fe/Mn ions were released, like site I, indicated that the reduction of organic matter with Fe/Mn oxides as electron acceptors occurred in the surface of the sediments. However, it is worth noting that other ions show large fluctuations within this range, which may be due to biological erosion.

The methane concentration in pore water at site Ⅱ decreased with increasing depth, from 120 μM at 625 cm to roughly 0 μM at 400 cm. The methane seepage intensity in the pore fluid was significantly higher than

sites I. Additionally, the methane flux diffused from sediments into seawater reached 15.9 mmol/m^2/yr, shown at Fig. 2. The sulfate concentration also decreased rapidly within 200–300 cm, indicating that AOM progress occurred here. The AOM took conducted at shallower sediment compared to sites I, which was another evidence of high seepage intensity. However, it is worth noting that below 300 cm depth of the sediment, the SO_4^{2-} concentration was not depleted at as typical for the SMTZ region with increasing depth, but instead increased to be comparable to the shallow surface layer. Combined with the characteristics of bubble plumes observed at the site Ⅱ, it was speculated that a fluid migration channel at this depth which could accelerated material exchange and circulation, lead to SO_4^{2-} concentration recovered. The DIC, Mg^{2+}, and Ca^{2+} concentration in the pore fluids vary less than those in the surface pore fluids in the same depth range, which was thought to be related to the same reason. The substance concentration profile in pore fluids of site Ⅱ was complicated by the peculiar geological structure. Carbonates make up 15.9% of the mineral composition of surface sediments, which was not a lot but was close to the 16.5% found in surface site I. This was because gravity column sampling site has specific requirements, and the hard carbonate crust is typically not chosen for gravity column sampling site. As large amounts of sulfide continue to be released, and as reactive iron was depleted in pore fluids, the continuously generated HS^- will accumulate and diffuse in the upper and lower layers to form a wider range of pyrite in sediment. Scanning Electron Microscopy (SEM) observed pyrite in the sediment at a depth of 625 cm, shown at Fig 5d, and relative Energy-dispersive x-ray spectroscopy (EDXS) spectrum also prove high sulfur and iron contents of the sediment. The result is that the distribution of pyrite in the surface sediments as well. Pyrite appeared is a crucial indicator of the oscillation of methane flux, and pyrite was produced across the range indicated that methane fluxes in the region did not change significantly over this time period [41]. Otherwise, iron-sulfide minerals represent the most important form of sulfur in sediment, iron-mediated sulfur burial controlled by AOM is also an important component of sulfur burial in marine sediments.

Massive methane seepage causes carbonate precipitates formed at the sediment-seawater interface through distinctive biogeochemical progresses. The hard substrata of methane-derived authigenic carbonate mounds were unsuitable for the *Vesicomyid* clams settlement, which requires soft sediments for absorbed sulphides [42]. Bathymodiolin mussels are rely primarily on methanotrophic symbionts, and they settlement in the zone of methane-rich fluid or sediment, supplying both methane and oxygen to commensal organisms and creating a stable environment for bacteria that helps them adapt to temporal and spatial variations [43]. Additionally, bathymodiolin mussels need to connect to hard substrata by byssus, like Carbonate crust [42]. Consequently, with the increased of methane flux through the sediment-water interface, bathymodiolin mussels be later successional species than *Vesicomyid* clams, and become the most abundant taxa, a thriving cold seep ecology developed.

In a word, site Ⅱ was in the cold seep stage of the high methane leakage intensity, suggested that the sediments were in a methane-rich environment and intensification of AOM, cause series of biogeochemical reactions, accelerated metal ion migration in pore fluid and sediment mineral formation, additional methane is likely to escape directly into the bottom waters and facilitating seep community development. At the sediment-seawater interface, a large number and variety of organisms thrive in this stage.

4. CONCLUSIONS

We thoroughly analyzed the intrinsic interactions of the succession sequence for seep communities and biogeochemical footprints of cold seep at various stages by observing and analyzing the ecosystem at the sediment-seawater interface of different methane leakage intensity regions, combining with the ion concentration profile in pore fluids and sediment composition of gravity column core. Our research demonstrates that in the early stage, the low methane flux at the sediment and biogeochemical processes in the sediment are good filters for methane emission. As the methane flux increases, the AOM in the sediment is enhanced, with the benthic community development and converts the released methane into carbonate rock to storage through biogeochemical processes. Based on the above analysis, we revealed the mechanism of the influence of different methane seepage intensities on the developmental stages of cold seep, and offerd valuable insights into biogeochemical footprints and ecosystem evolution cold seeps. Our research reveals the mechanisms of the marine methane carbon cycle and contributed to the understanding and development of NGH resources in marine and has implications for climate change regulation.

ACKNOWLEDGEMENT

The authors would like to acknowledge the financial support for this research received from the National Natural Science Foundation of China (42022046,

41890850), the National Key Research and Development Program (2021YFF0502300), Guangdong Natural Resources Foundation, (GDNRC[2022]45), Guangzhou Science and Technology Project (202102020971), and Guangdong Provincial Key Laboratory Project (2019B121203011).

REFERENCE

[1] Piñero E, Marquardt M, Hensen C, Haeckel M, Wallmann K. Estimation of the global inventory of methane hydrates in marine sediments using transfer functions. Biogeosciences. 2013;10:959-75.
[2] Church J, Clark P, Cazenave A, Gregory J, Jevrejeva S, Levermann A, et al. Climate Change 2013: The Physical Science Basis. Contribution of Working Group I to the Fifth Assessment Report of the Intergovernmental Panel on Climate Change. Sea Level Change. 2013:1138-91.
[3] Knoblauch C, Beer C, Liebner S, Grigoriev MN, Pfeiffer EMJNCC. Methane production as key to the greenhouse gas budget of thawing permafrost. 2018;8:309-12.
[4] Feng J-C, Yan J, Wang Y, Yang Z, Zhang S, Liang S, et al. Methane mitigation: Learning from the natural marine environment. The Innovation. 2022;3:100297.
[5] Ruppel CD, Kessler JD. The interaction of climate change and methane hydrates. Reviews of Geophysics. 2017;55:126-68.
[6] Zachos JC, Röhl U, Schellenberg SA, Sluijs A, Hodell DA, Kelly DC, et al. Rapid Acidification of the Ocean During the Paleocene-Eocene Thermal Maximum. 2005;308:1611-5.
[7] Dawson AG, Long D, Smith DE. The Storegga Slides: Evidence from eastern Scotland for a possible tsunami. Marine Geology. 1988;82:271-6.
[8] Young RW, Bryant EA. Catastrophic wave erosion on the southeastern coast of Australia: Impact of the Lanai tsunamis ca. 105 ka? Geology. 1992;20:199-202.
[9] Knittel K, Boetius A. Anaerobic oxidation of methane: progress with an unknown process. Annual review of microbiology. 2009;63:311-34.
[10] Borowski WS, Paull CK, Ussler W. Global and local variations of interstitial sulfate gradients in deep-water, continental margin sediments: Sensitivity to underlying methane and gas hydrates. Marine Geology. 1999;159:131-54.
[11] Boetius A, Ravenschlag K, Schubert CJ, Rickert D, Widdel F, Gieseke A, et al. A marine microbial consortium apparently mediating anaerobic oxidation of methane. Nature. 2000;407:623-6.
[12] Orphan VJ, House CH, Hinrichs KU, McKeegan KD, DeLong EF. Methane-consuming archaea revealed by directly coupled isotopic and phylogenetic analysis. Science. 2001;293:484-7.
[13] Jørgensen BB. Mineralization of organic matter in the sea bed—the role of sulphate reduction. Nature. 1982;296:643-5.
[14] Jørgensen BB, Beulig F, Egger M, Petro C, Scholze C, Røy H. Organoclastic sulfate reduction in the sulfate-methane transition of marine sediments. Geochimica et Cosmochimica Acta. 2019;254:231-45.
[15] Zhang Y, Luo M, Hu Y, Wang H, Chen D. An Areal Assessment of Subseafloor Carbon Cycling in Cold Seeps and Hydrate-Bearing Areas in the Northern South China Sea. Geofluids. 2019;2019:1-14.
[16] Wang X, Li N, Feng D, Hu Y, Bayon G, Liang Q, et al. Using chemical compositions of sediments to constrain methane seepage dynamics: A case study from Haima cold seeps of the South China Sea. Journal of Asian Earth Sciences. 2018;168:137-44.
[17] Feng J, Yang S, Wang H, Liang J, Fang Y, Luo M. Methane Source and Turnover in the Shallow Sediments to the West of Haima Cold Seeps on the Northwestern Slope of the South China Sea. Geofluids. 2019;2019:1010824.
[18] Hu Y, Luo M, Liang Q, Chen L, Feng D, Yang S, et al. Pore fluid compositions and inferred fluid flow patterns at the Haima cold seeps of the South China Sea. Marine and Petroleum Geology. 2019;103:29-40.
[19] Ke Z, Li R, Chen Y, Chen D, Chen Z, Lian X, et al. A preliminary study of macrofaunal communities and their carbon and nitrogen stable isotopes in the Haima cold seeps, South China Sea. Deep Sea Research Part I: Oceanographic Research Papers. 2022;184:103774.
[20] Li N, Feng D, Wan S, Peckmann J, Guan H, Wang X, et al. Impact of methane seepage dynamics on the abundance of benthic foraminifera in gas hydrate bearing sediments: New insights from the South China Sea. Ore Geology Reviews. 2021;136:104247.
[21] Liu W, Wu Z, Xu S, Wei J, Peng X, Li J, et al. Pore-water dissolved inorganic carbon sources and cycling in the shallow sediments of the Haima cold seeps, South China Sea. Journal of Asian Earth Sciences. 2020;201:104495.
[22] Wei J, Li J, Wu T, Zhang W, Li J, Wang J, et al. Geologically controlled intermittent gas eruption and its impact on bottom water temperature and chemosynthetic communities—A case study in the “HaiMa” cold seeps, South China Sea. 2020;55:6066-78.
[23] Xin Y, Wu N, Sun Z, Wang H, Chen Y, Xu C, et al. Methane seepage intensity distinguish microbial communities in sediments at the Mid-Okinawa Trough. The Science of the total environment. 2022;851:158213.
[24] Xu H, Du M, Li J, Zhang H, Chen W, Wei J, et al. Spatial distribution of seepages and associated biological communities within Haima cold seep field, South China Sea. Journal of Sea Research. 2020;165:101957.
[25] Peketi A, Mazumdar A, Joao HM, Patil DJ, Usapkar A, Dewangan P. Coupled C–S–Fe geochemistry in a rapidly accumulating marine sedimentary system: Diagenetic and depositional implications. 2015;16:2865-83.
[26] Sun Q, Cartwright J, Lüdmann T, Wu S, Yao G. Three-dimensional seismic characterization of a complex sediment drift in the South China Sea: Evidence for unsteady flow regime. 2017;64:832-53.
[27] Liang Q, Hu Y, Feng D, Peckmann J, Chen L, Yang S, et al. Authigenic carbonates from newly discovered active cold seeps on the northwestern slope of the South China Sea: Constraints on fluid sources, formation environments, and seepage dynamics. Deep Sea Research Part I: Oceanographic Research Papers. 2017;124:31-41.
[28] Liu B, Chen J, Yang L, Duan M, Liu S, Guan Y, et al. Multi-beam and seismic investigations of the active Haima cold seeps, northwestern South China Sea. Acta Oceanologica Sinica. 2021;40:183-97.

[29] Sun X, Turchyn AV. Significant contribution of authigenic carbonate to marine carbon burial. Nature Geoscience. 2014;7:201-4.
[30] Boudreau BP. Diagenetic Models and Their Implementation: Modelling Transport and Reactions in Aquatic Sediments. 1996.
[31] Hubbard CR, Snyder RL. RIR - Measurement and Use in Quantitative XRD. Powder Diffraction. 1988;3:74-7.
[32] Boulay S, Colin C, Trentesaux A, Frank N, Liu Z. Sediment sources and East Asian monsoon intensity over the last 450 ky. Mineralogical and geochemical investigations on South China Sea sediments. Palaeogeography, Palaeoclimatology, Palaeoecology. 2005;228:260-77.
[33] Hensen C, Wallmann K, Schmidt M, Ranero CR, Suess E. Fluid expulsion related to mud extrusion off Costa Rica—A window to the subducting slab. Geology. 2004;32:201-4.
[34] Lu Y, Sun X, Xu H, Konishi H, Lin Z, Xu L, et al. Formation of dolomite catalyzed by sulfate-driven anaerobic oxidation of methane: Mineralogical and geochemical evidence from the northern South China Sea. American Mineralogist. 2018;103:720-34.
[35] Arndt S, Jørgensen BB, LaRowe DE, Middelburg JJ, Pancost RD, Regnier P. Quantifying the degradation of organic matter in marine sediments: A review and synthesis. Earth-Science Reviews. 2013;123:53-86.
[36] Hensen C, Zabel M, Pfeifer K, Schwenk T, Kasten S, Riedinger N, et al. Control of sulfate pore-water profiles by sedimentary events and the significance of anaerobic oxidation of methane for the burial of sulfur in marine sediments. Geochimica et Cosmochimica Acta. 2003;67:2631-47.
[37] Coffin RB, Hamdan LJ, Smith JP, Rose PS, Plummer RE, Yoza B, et al. Contribution of Vertical Methane Flux to Shallow Sediment Carbon Pools across Porangahau Ridge, New Zealand. 2014;7:5332-56.
[38] Borowski WS, Rodriguez NM, Paull CK, Ussler W. Are 34S-enriched authigenic sulfide minerals a proxy for elevated methane flux and gas hydrates in the geologic record? Marine and Petroleum Geology. 2013;43:381-95.
[39] Neretin LN, Böttcher ME, Jørgensen BB, Volkov II, Lüschen H, Hilgenfeldt K. Pyritization processes and greigite formation in the advancing sulfidization front in the upper Pleistocene sediments of the Black Sea 1 1Associate editor: D. Canfield. Geochimica et Cosmochimica Acta. 2004;68:2081-93.
[40] Wilkin RT, Barnes HL. Pyrite formation by reactions of iron monosulfides with dissolved inorganic and organic sulfur species. Geochimica et Cosmochimica Acta. 1996;60:4167-79.
[41] Lim YC, Lin S, Yang TF, Chen Y-G, Liu C-S. Variations of methane induced pyrite formation in the accretionary wedge sediments offshore southwestern Taiwan. Marine and Petroleum Geology. 2011;28:1829-37.
[42] Olu K, Sibuet M, Harmegnies F, Foucher JP, Fiala-Médioni A. Spatial distribution of diverse cold seep communities living on various diapiric structures of the southern Barbados prism. Progress in Oceanography. 1996;38:347-76.
[43] Petersen JM, Dubilier N. Methanotrophic symbioses in marine invertebrates. 2009;1:319-35.